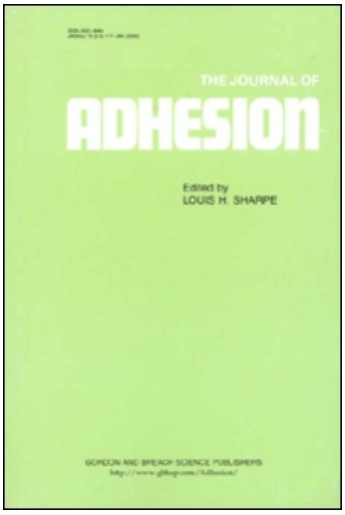

The Journal of Adhesion
Publication details, including instructions for authors and subscription information:
http://www.informaworld.com/smpp/title~content=t713453635

Numerical Analysis of a Thick-Adherend Lap Shear Specimen

M. Y. Tsai[ab]; J. Morton[c]; D. W. Oplinger[d]
[a] Department of Engineering Science and Mechanics, Virginia Polytechnic Institute and State University Blacksburg, VA, USA [b] Tjing Ling Industrial Research Institute, National Taiwan University, Taipei, Taiwan, R. O. C. [c] Structural Materials Center, DRA, Farnborough, GU, UK [d] Federal Aviation Administration Technical Center, NJ, USA

To cite this Article Tsai, M. Y. , Morton, J. and Oplinger, D. W.(1997) 'Numerical Analysis of a Thick-Adherend Lap Shear Specimen', The Journal of Adhesion, 62: 1, 257 — 280
To link to this Article: DOI: 10.1080/00218469708014572
URL: http://dx.doi.org/10.1080/00218469708014572

J. Adhesion, 1997, Vol. 62, pp. 257–280
Reprints available directly from the publisher
Photocopying permitted by license only

Numerical Analysis of a Thick-Adherend Lap Shear Specimen

M. Y. TSAI[a,*], J. MORTON[b] and D. W. OPLINGER[c]

[a]*Department of Engineering Science and Mechanics, Virginia Polytechnic Institute and State University, Blacksburg, VA 24061-0219, USA;*
[b]*Structural Materials Center, DRA, Farnborough, Hampshire, GU 14 6TD, UK;*
[c]*Federal Aviation Administration Technical Center, Atlantic City International Airport, NJ 08405, USA*

(Received 1 July 1996; In final form 18 December 1996)

A finite element stress analysis of a thick-adherend lap shear specimen to determine the adhesive shear properties is performed. Key problems associated with this test specimen include the non-uniformity of adhesive stress fields, load eccentricity effects and other less well-characterized mechanics. The numerical model, validated by comparing with the moiré experiment, is proposed for investigation of these problems. Full-field non-uniform stress distributions in the test region are presented. The obtained adhesive shear stress distributions are compared with those from the moiré experiment and the classical theoretical solutions. It is shown that the present two-dimensional solutions agree well with experimental solutions while the theoretical solutions based on simple assumptions differ from those from the numerical and experimental analyses. Load eccentricity encountered in the experimental tests is investigated. It is shown that load eccentricity greatly affects the adhesive shear stress distributions, but not the stress state at the center point of the bond line. Thus, load eccentricity effects would cause large data scatter in adhesive shear modulus and strength measurement. The effect of the adhesive/adherend elastic modulus ratio on the adhesive stress distributions is also investigated. Correction factors accounting for non-uniformity of the adhesive shear stress distributions are determined and used to determine the adhesive shear modulus from the experimental data.

Keywords: Lap-shear test; adhesive joint; adhesive shear properties; KGR-1 extensometer; finite element; stress analysis

*Corresponding author. Present address: Tjing Ling Industrial Research Institute, National Taiwan University, 130 Keelung Road, Sec. III, Taipei, Taiwan, R.O.C.

INTRODUCTION

Adhesive bonding technology has gained the attention of the automotive, aerospace, wood, plastics as well as the electronic packaging industries. When a thin-layer adhesive is used in bonding load-bearing structures, the adhesive is usually designed to carry shear loading. Adhesive material shear properties (such as modulus, strength or full stress-strain curves), especially for *in-situ* properties under the different temperatures and environments, are then needed in both structural design and analysis.

A simple, reliable and robust test method is required for the determination of adhesive shear properties. An adhesive shear specimen with a thick adherend using the KGR-1 extensometer, proposed by Krieger, is one of the most popular test methods for determining thin-layer adhesive shear stress-strain response [1–3]. The configuration and dimensions of the test specimen are shown in Figure 1(a). The test specimen has a 2c-long overlap test section which is located at the center of the specimen that is produced by machining two slots, one at the upper adherend and the other at the lower one, and separated by 2c. The specimen is loaded in tension through pins. The adhesive in the 2c-long bond line is subjected to the shear force. A KGR-1 extensometer was used to measure the relative shear deformation between two points which are symmetrically located on each side of the bond line. The shear deformations recorded by the extensometer include the shear deformations of the adherends which can be determined by testing a dummy specimen (a specimen without an adhesive layer). The adhesive shear deformation can be obtained by subtracting the shear deformation of the dummy specimen from the total shear deformation of the test specimen, as indicated in Figure 1(b) which contains typical adhesive shear stress-strain response from a KGR-1 extensometer.

It has been proposed in the literature [2, 4, 5] that the thick-adherend test specimen does not produce an uniform adhesive shear stress (or strain) distribution along the entire bond line, within the material linear-elastic range. It has been suggested in Krieger's test procedure [1] that the adhesive shear strain measured at the quarter-point of the bond line is close to that of the average shear stress, which is obtained by simply dividing the applied force by the bond area.

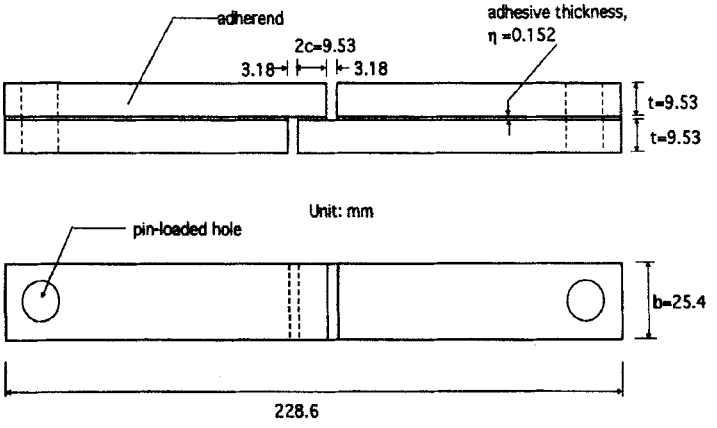

(a)

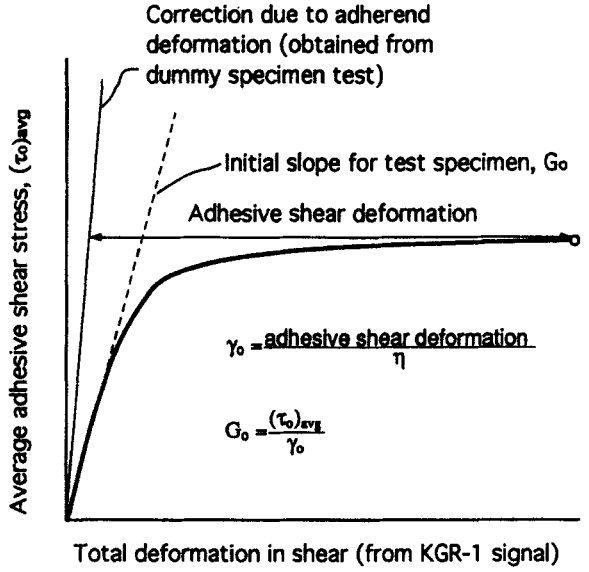

(b)

FIGURE 1 (a) Configuration and dimensions of a thick-adherend lap shear specimen. (b) Typical adhesive shear stress-strain curve measured by KGR-1 extensometer.

However, the test specimen when loaded in tension is sensitive to a load eccentricity caused by the thick adherend and pin-loading mechanism. Figure 2 shows typical strain gage responses for a test specimen under the tensile load. It is apparent that, for eccentric loading, strains recorded in gages 1 and 3 are tensile, while strains in gages 2 and 4 are compressive. The load eccentricity can be greatly reduced by using the notched pins as observed by Tsai and *et al.* [5] in strain gage and moiré experiments. Load eccentricity would result in a large scatter in adhesive shear modulus data and premature failure of the specimen [5]. Tsai *et al.* [6] have also shown that strain gage measurement, with a properly defined correction factor to allow for stress non-uniformity, can be used to determine the thin-layer adhesive shear modulus, provided that the stress (or strain) fields in the specimen's test section are

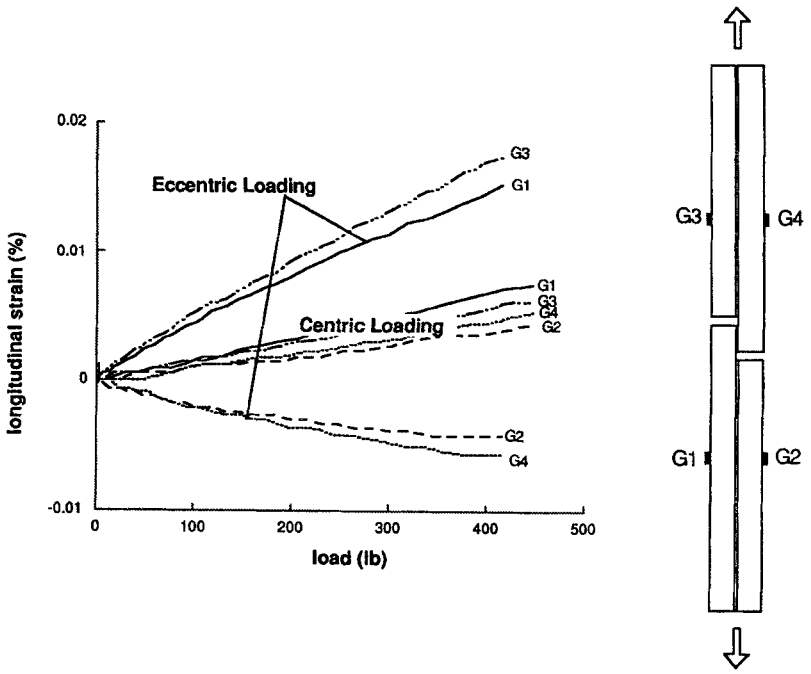

FIGURE 2 Strain gage responses to load eccentricity, observed in the thick-adherend lap shear specimen, due to inappropriate loading.

well characterized. With both the KGR-1 extensometer and the strain gage technique, the non-uniformity of stress fields in the specimen's test section and the load eccentricity effects need to be examined.

The objectives of this study are to provide a numerical model for the stress analysis of the KGR-1 adhesive shear specimen, to validate the model by comparing experimental and theoretical analyses, to study the mechanics of the test specimen with regard to the effects of load eccentricity and adhesive material properties on the adhesive stress distributions, and to provide suggestions for accurate measurement of adhesive shear modulus.

NUMERICAL MODEL

Two-dimensional linear elastic finite element analyses using the ABAQUS code [7] have been performed. Transverse deflections, resulting from the bending moment due to the discontinuity of the neutral axis, are small and negligible due to the large bending rigidity of the thick adherends. As a result, the stretching of the adherends is uncoupled from the transverse deflection. That is, unlike the thin-adherend single-lap joint [8], geometrically nonlinear effects are negligible. The geometry and boundary conditions for the finite element model are shown in Figure 3. The length of the outer parts has been modeled as 19 mm (0.75 inch), rather than the actual length of 95.3 mm (3.75 inch). These short outer parts reduced the total elements in the numerical calculation without sacrificing the accuracy of results for the test section. The boundary conditions applied were a hinge at one end, and a roller (constrained in the vertical direction) and horizontal applied force per unit width, T, at the other. For the case without load eccentricity, these boundary conditions are placed at the center line of the specimen, while these boundary conditions are shifted up (or down) away from the center line for the case with load eccentricity.

A linear-elastic plane strain model was used in the finite element analysis. For the adherend properties, elastic modulus $E_s = 70$ GPa and Poisson's ratio $\nu = 0.33$. For the adhesive, elastic modulus $E_o = 2.17$ GPa (or $G_o = 0.83$ GPa) and Poisson's ratio $\nu_o = 0.31$. Since the adhesive layer is relatively very thin compared with the thickness of the adherends, adhesive stress variation through the thickness is

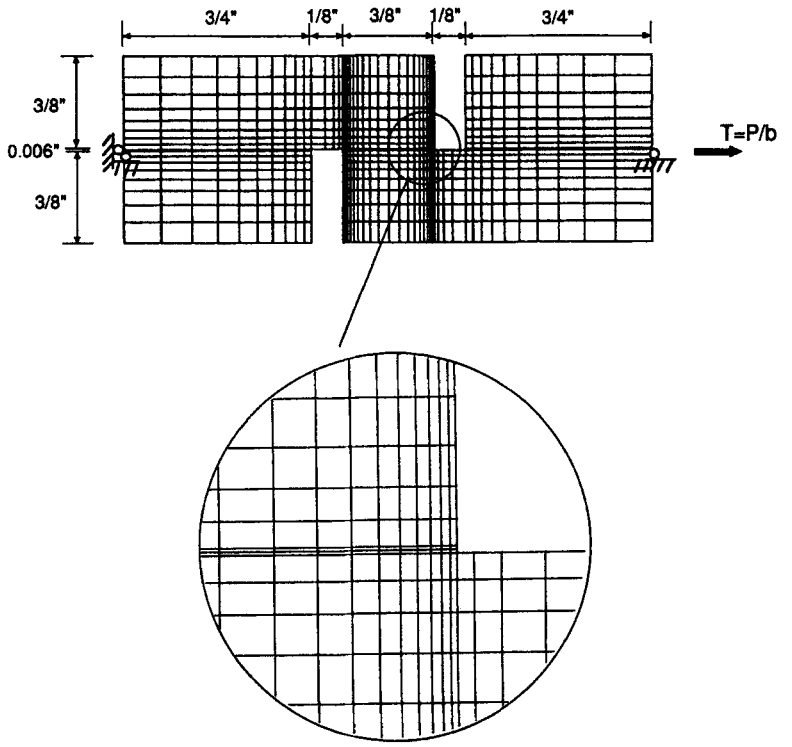

FIGURE 3 Geometry, mesh, and boundary conditions used in the finite element analysis.

negligible. In addition, the stress components (except the longitudinal normal one) is continuous across the interface between the adherend and adhesive. Two constant-stress elements were used across the thickness of the adhesive layer. The size of the adhesive element gets smaller upon approaching the end of the overlap where large stress gradients occur. Because there were two constant-stress elements across the adhesive, and the stress values at the nodal points are determined by averaging the values from adjacent elements, the values of adhesive stresses along the center line of the adhesive are approximately equal to the average values across the thickness of the adhesive layer. Theoretical stress singularities in very localized regions (with a distance in the order of thickness of adhesive) such reentrant corners or interface corners are neglected in the present analysis.

In order to validate the numerical model, the adhesive and adherend stress distributions obtained from the finite element analysis and moiré experiment [5] for the case without load eccentricity, are compared and shown in Figure 4. The stress components are normalized by the average adhesive shear stress, $(\tau_o)_{avg}(=T/2c)$. It is apparent that the adhesive shear distributions from both the numerical and experimental results are in good agreement. Also, the adherend longitudinal stress distributions along the middle line of the bridge are in reasonably good agreement in the numerical analysis and experiment. This implies that the finite element model used in this study is appropriate for modeling the mechanics of the test specimen.

A parametric study of the test specimen is conducted in this numerical analysis. Parameters such as the adhesive/adherend elastic modulus ratio (E_o/E_s) and load eccentricity are investigated. Correction factors taking account of the adhesive shear non-uniformity are calculated at the middle point of the bond line for various E_o/E_s. The load eccentricity effect on the adhesive stress distribution is also investigated.

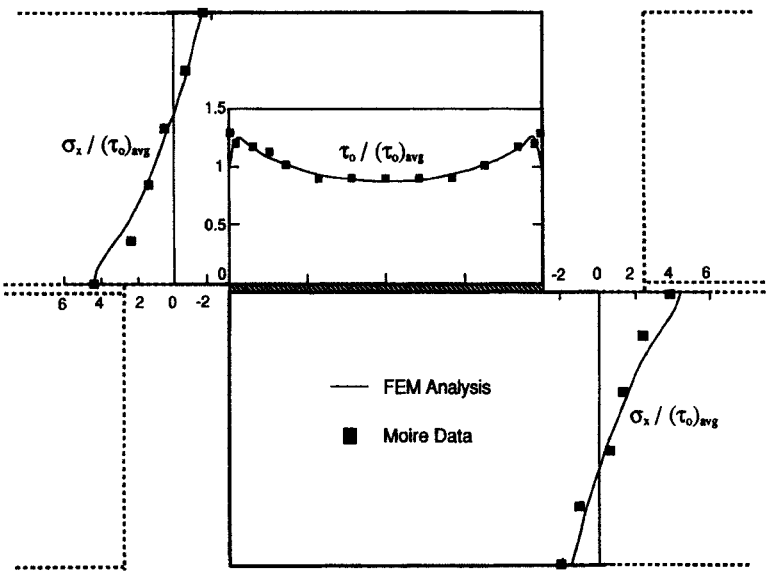

FIGURE 4 Verification of the numerical model by comparing the obtained adherend longitudinal normal and adhesive shear stresses with those from the moiré experiment.

THEORIES

There are two classical solutions available for single-lap joints: one developed by Volkersen in 1938 [9], and the other proposed by Goland and Reissner in 1944 [8].

Volkersen's solution is a simple shear lag solution based on the assumption of bar-like adherends bonded through a shear-deformable adhesive layer. That is, the adherends carry only longitudinal force which causes elongation uniformly across the thickness of the adherends. This model can be used to analyze unbalanced joints in which E_1t_1 (elastic modulus times thickness in the upper adherend) is not equal to E_2t_2 (in the lower adherend). The normalized adhesive shear stress is given by

$$\frac{\tau_o}{(\tau_o)_{\text{avg}}} = A\sinh(\beta x) + B\cosh(\beta x)$$

where

$$A = \frac{\beta c}{\cosh(\beta c)}\left[\frac{1-\dfrac{E_2t_2}{E_1t_1}}{1+\dfrac{E_2t_2}{E_1t_1}}\right];$$

$$B = \frac{\beta c}{\sinh(\beta c)};$$

$$\text{and } \beta^2 = \frac{G_o}{\eta}\left(\frac{1}{E_1t_1}+\frac{1}{E_2t_2}\right)$$

The average shear stress, $(\tau_o)_{\text{avg}}$, is equal to $T/2c$.

On the other hand, Goland and Reissner present a beam-on-elastic-foundation model in Part III of their paper. The adherends are modeled as beams (or cylindrical bent plates) taking into account the adherend longitudinal force, bending moment and shear. The adhesive layer is modeled as a shear plus transverse normal spring. The model is valid for balanced joints in which $E_1 = E_2 = E$, and $t_1 = t_2 = t$. The

normalized adhesive shear stress is

$$\frac{\tau_o}{(\tau_o)_{\text{avg}}} = -\frac{1}{4}\left[\frac{\beta c}{t}(1+3k)\frac{\cosh\left(\frac{\beta c}{t}\frac{x}{c}\right)}{\sinh\frac{\beta c}{t}} + 3(1-k)\right]$$

where the normalized edge moment, k, is equal to $2M_o/Tt$, and

$$\beta^2 = \frac{8tG_o}{E\eta}$$

The M_o here denotes the moment acting at the end of the overlap.

RESULTS AND DISCUSSION

Stress Distributions

The deformation and stress distributions (normalized by the average adhesive shear stress) for the test specimen under ideal loading (without load eccentricity) are shown in Figure 5. The deformed shape in Figure 5(a) shows that the upper adherend near the end of the overlap bends concave-up in the y-direction, while the lower adherend deforms concave-down. Also, the adhesive layer has much larger shear deformation than the adherend regions adjacent to the adhesive, although the shear stress states in the adhesive and in those adherend regions are similar. That is attributed to the greater shear compliance in the adhesive than in the adherend. The normalized longitudinal normal (σ_x), transverse normal (σ_y), and shear (τ_{xy}) stress contours are shown in Figures 5(b), (c) and (d), respectively. It is apparent that σ_x is a dominant component of the stress state in the adherend. The greatest σ_x occurs at the corner at the end of the overlap where maximum bending moment appears. This bending moment resulting from the discontinuity of the neutral axis affects the entire overlap region, such that no uniform σ_x distribution across the thickness of the overlap is observed. The nature of the σ_x discontinuity due to the material discontinuity occurs at the interface between the adhesive

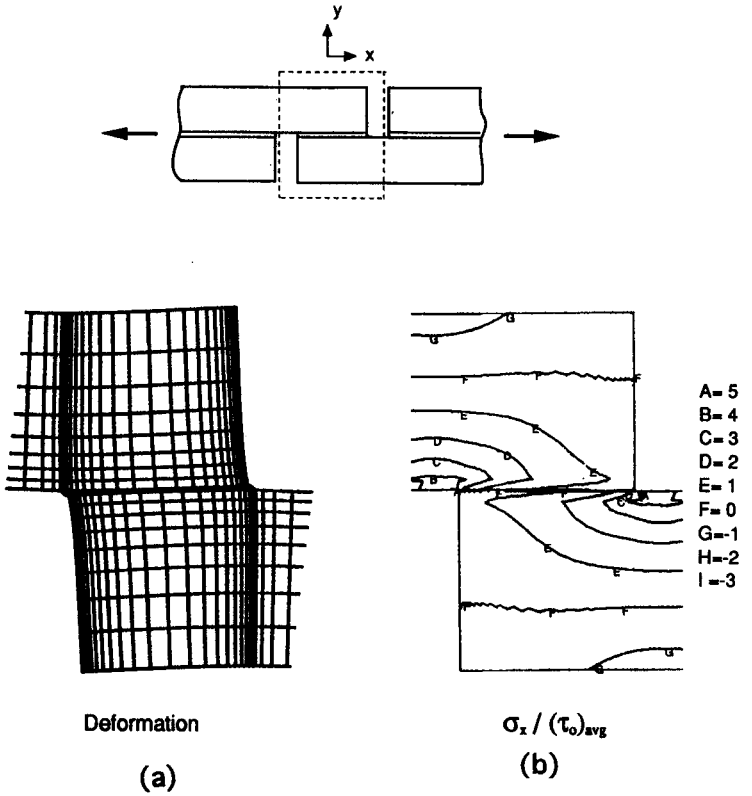

FIGURE 5 (a) Deformed shape, (b) normalized longitudinal normal stress distribution, (c) normalized transverse normal stress distribution, (d) normalized shear stress distribution for the test specimen loaded *without eccentricity*.

and adherend. The distributions for σ_y and τ_{xy}, however, are continuous across the adhesive/adherend interface. It is also observed that τ_{xy} is non-uniform along the bond line. However, at and near the center of the bond line there is a small region with an approximately uniform shear stress.

The adhesive shear stress distribution obtained from the finite element analysis, shown in Figure 6, is compared with those from the moiré experiment and theoretical predictions. It is clear that the two-dimensional finite element solution is in a good agreement with moiré results, but not with the theoretical solutions. Goland and Reissner's

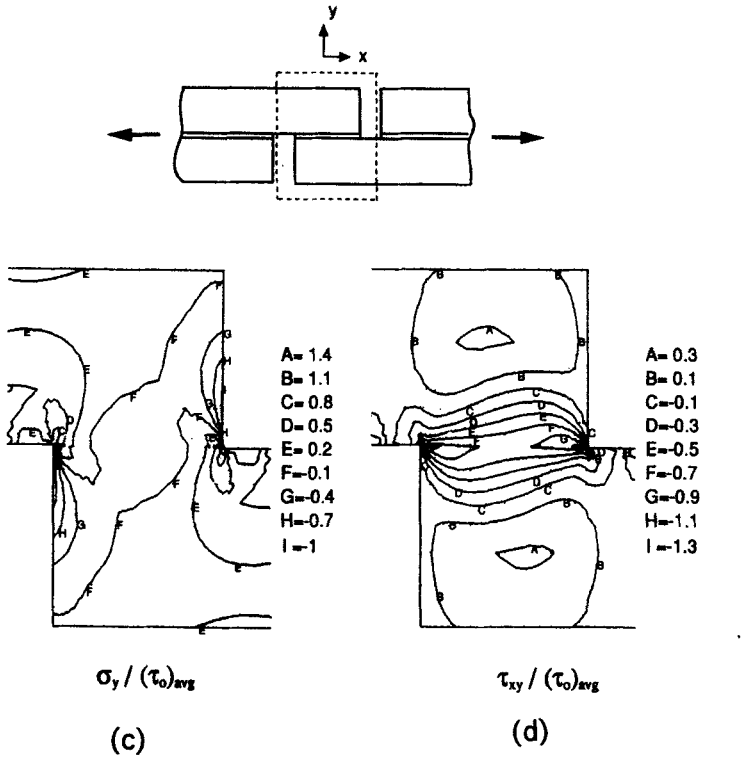

FIGURE 5 (Continued).

solution with the edge moment, M_o, over-predicts the maximum adhesive shear stress, while Volkersen's solution under-predicts it. It is noted that Volkersen's solution is based on the shear lag approach which neglects the adherend bending moment, while Goland and Reissner, in their Part III analysis, model the adherends as beams which include bending moment and shear. Since adherend shear does not affect the adhesive shear stress in the Goland and Reissner solution, Volkersen's solution can be recovered from the Goland and Reissner solution by assuming no adherend moment, shown in Figure 6. It is also shown that theoretical solutions based on a one-dimensional analysis provide a poor approximation to the solutions of the present two-dimensional case in which the adherends in the overlap region have an aspect ratio about 1. It has been demonstrated that

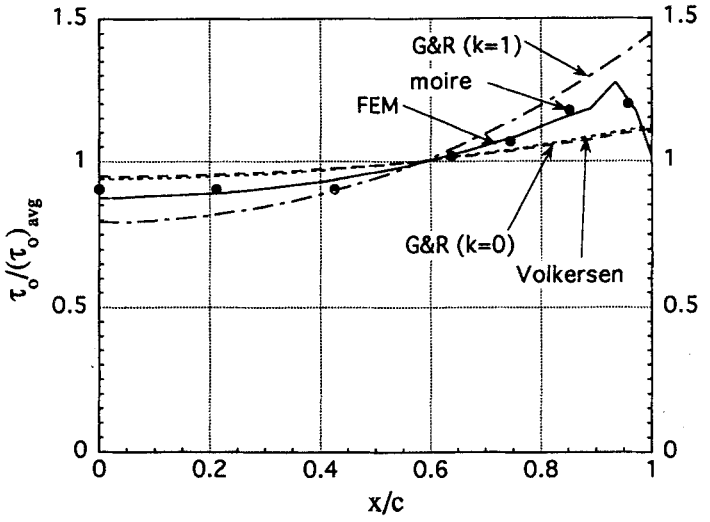

FIGURE 6 Comparisons of normalized adhesive shear stress distributions obtained from the 2-D finite element analysis (FEM), moiré experiment, Volkersen's solution and Goland and Reissner's solution (G&R). Note $k = 2\ M_o/Tt$.

the modified Goland and Reissner solution including adherend shear deformation gives a better prediction for this two-dimensional case [10].

Since the results of a dummy specimen are used to adjust the results of the test specimen [1,6], an understanding of the mechanics of the dummy specimen is essential. The deformed shape is very similar to that of the test specimen except for a local region in the virtual bond line where the dummy specimen has a stiffer shear modulus and, thus, less shear deformation than the test specimen. Unlike the test specimen, there is no σ_x discontinuity for the dummy specimen in the same region as the adhesive layer in the test specimen. The stress concentrations and gradients for the three stress components are larger than those in the test specimen. The regions with high stress gradients are confined to very small areas near and at the corner at the end of the overlap. Theoretically, the corner with 270° vertex angle has a stress singularity, based on linear elastic theory [11]. This stress singularity will generate theoretically-unbounded stress values. In practice these stresses are, however, bounded by a local geometric feature or plastic deformation.

Load Eccentricity Effect

There is an eccentricity problem when the specimen is loaded with the usual pins and this load eccentricity significantly affects the stress distributions and deformations in the test section. Load eccentricity investigated in the present analysis is based on the real situation encountered in the experiments. An example of the deformed shape and stress distributions are shown in Figure 7 for a test specimen loaded with an eccentricity 0.44 × thickness of the adherend from the center line of the specimen to the upper adherend. The deformed shape illustrated in Figure 7(a) indicates that the upper adherend in

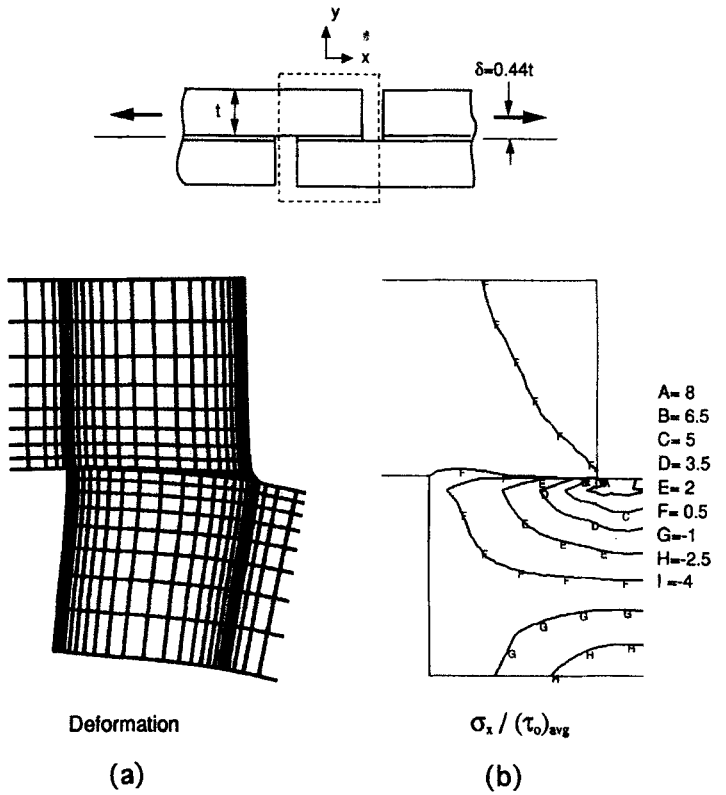

FIGURE 7 (a) Deformed shape, (b) normalized longitudinal normal stress distribution, (c) normalized transverse normal stress distribution, (d) normalized shear stress distribution for the test specimen loaded *with eccentricity*.

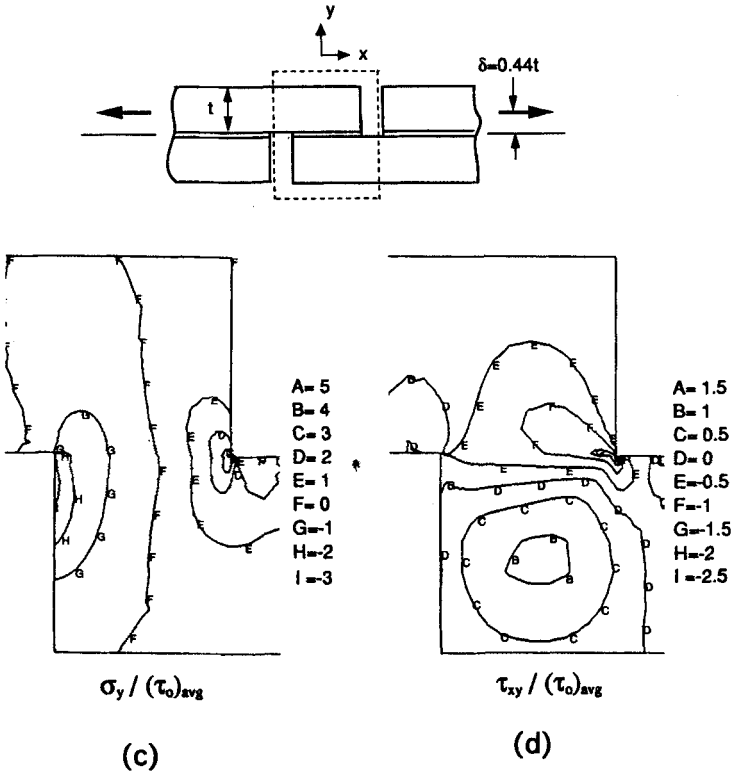

FIGURE 7 (Continued).

the test section has less bending deformation than the lower adherend. The adhesive layer near and at the right-side corner suffers larger shear deformation than at the left-side corner. The antisymmetrical deformation does not occur in this case with load eccentricity. Figure 7(b) indicates that the lower adherend carries large bending stresses, but not the upper adherend. The maximum values of σ_x, σ_y and τ_{xy} occur only at the right-side corner and, especially for σ_y, are much larger than those for the specimen with centric loading.

The effects of the load eccentricity on the adhesive stress distributions (for σ_{xo}, σ_{yo}, and τ_o) are shown in Figure 8 for cases with eccentricity $\delta = 0$ to $0.44t$. Note that the load eccentricity (off from the center toward one side) simulated here is typically encountered in

the experimental tests. The adhesive stresses in Figure 8 represent the average stress over the thickness of the adhesive. The τ_o distribution shown in Figure 8(a) is symmetric with respect to the axis $x = 0$ (the middle line of the overlap) for $\delta = 0$ (the case without load eccentricity). The adhesive shear stresses in the quarter-points of the bond line (*i.e.* $x/c = -0.5$ or 0.5) are approximately equivalent to the values averaged over the entire bond line. That is, $\tau_o \cong (\tau_o)_{avg}$. When δ increases, τ_o increases on one side and decreases on the other. If shear strain is measured at the quarter point, the strain might correspond to the average shear stress for the case without load eccentricity ($\delta = 0$), or to 1.2 times the average shear stress for the case with $\delta = 0.44t$ to

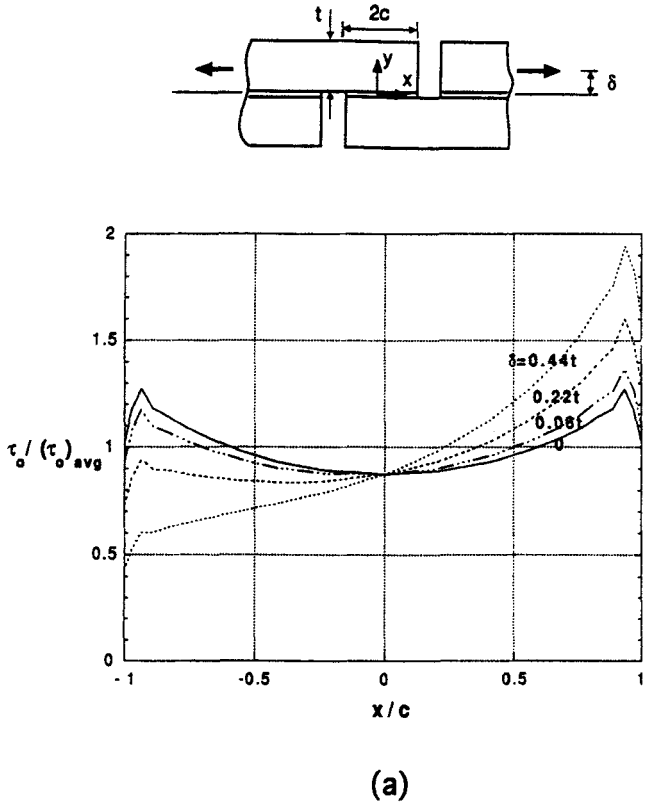

FIGURE 8 The effect of the load eccentricity on (a) adhesive shear stresses, (b) adhesive longitudinal normal stresses and (c) adhesive transverse normal stresses.

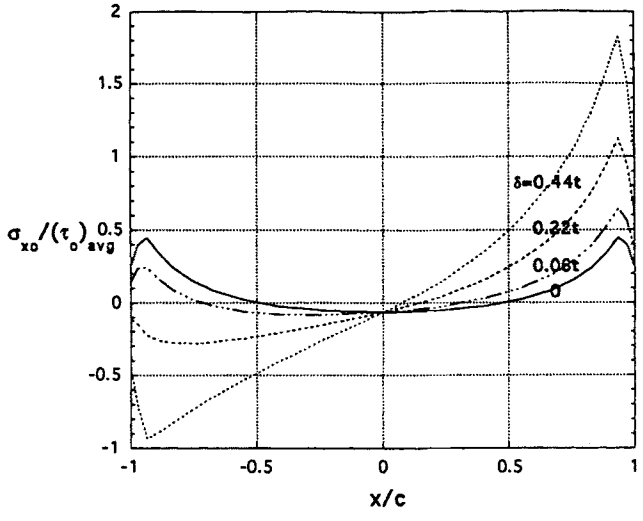

(b)

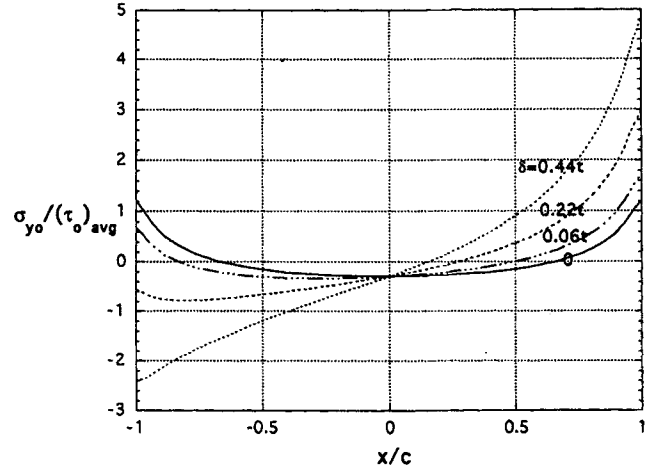

(c)

FIGURE 8 (Continued).

the upper adherend, or to 0.72 times the average shear stress with $\delta = 0.44t$ to the lower adherend. Thus, quarter-point measurement is very sensitive to load eccentricity. However, the shear strain measurement at the middle point of the bond line can eliminate the load eccentricity effect, but this requires a correction factor to correlate the shear stress at the middle point to the average shear stress. In Figure 8(b), for $\delta = 0$, σ_{xo} is small and compressive in the middle region, but large and tensile near both ends. With increasing δ, tensile stress increases at one side and decreases (or even becomes compressive) at the other. For σ_{yo} in Figure 8(c), the adhesive peel stress distributions have similar shapes to σ_{xo}, except for the stress values and the stress drop near the end of the overlap for σ_{xo} in order to satisfy the free boundary. An adhesive bending moment $M (M = \int_{-c}^{c} \sigma_{yo} x \, dx)$ on the adhesive is dependent on the eccentricity. The relationship between the adhesive bending moment and eccentricity will be discussed later using free body diagrams. For $\delta = 0$, maximum adhesive stresses for the three components are $\sigma_{xo} = 0.45(\tau_o)_{\text{avg}}$, $\sigma_{yo} = 1.2(\tau_o)_{\text{avg}}$, and $\tau_o = 1.25(\tau_o)_{\text{avg}}$. The adhesive shear and peel stresses seem to be predominant. However, for $\delta = 0.44t$ maximum adhesive stresses reach $\sigma_{xo} = 1.8(\tau_o)_{\text{avg}}$, $\sigma_{yo} = 4.8(\tau_o)_{\text{avg}}$, and $\tau_o = 1.9(\tau_o)_{\text{avg}}$. Then the adhesive peel stress would play an important role in failure initiation. As a result, premature adhesive failure would possibly occur. Thus, load eccentricity influences not only the adhesive shear modulus measurement which is based on the stress distribution, but also the adhesive shear strength determination.

To illustrate the fundamental machanics of the test specimen, free body diagrams are shown in Figures 9(a) and (b) representing the specimen under centric and eccentric loads, respectively. The V in Figure 9 denotes the adhesive shear force per unit width, *i.e.* $V = \int_{-c}^{c} \tau_o \, dx$. For the case without load eccentricity in Figure 9(a), the applied force, T, is equal to the adhesive shear. The self-equilibrium adhesive moments M_1 and M_2 ($M_1 = \int_{-c}^{0} \sigma_{yo} x \, dx$, $M_2 = \int_{-c}^{c} \sigma_{yo} x \, dx$) are equal and in opposite direction, and generate tensile adhesive peel stresses at the ends of the overlap. On the other hand, for the case with load eccentricity δ in Figure 9(b) an additional adhesive moment, M, is created by eccentric loading. The value of the M is equivalent to $T\delta$ based on the moment equilibrium. Thus, the adhesive peel stress distributions are constructed by the superposition of σ_{yo} from the moments M, M_1 and M_2.

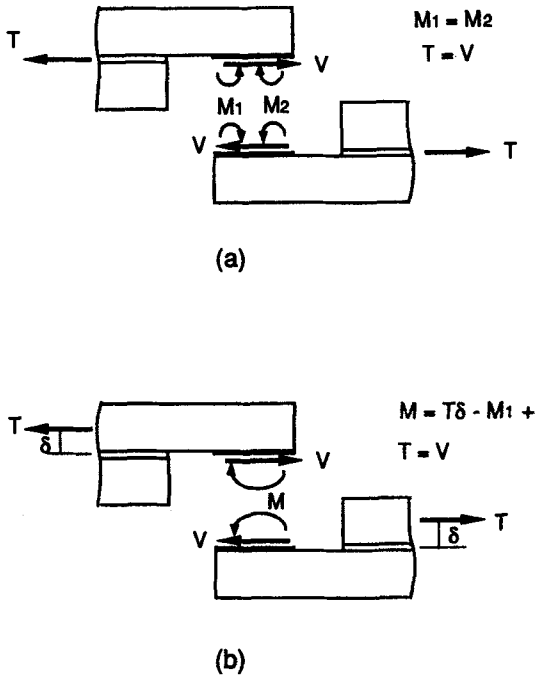

FIGURE 9 Free body diagrams for the test specimen loaded (a) without eccentricity, (b) with eccentricity δ.

Materials Property Dependence

The dependence of the adhesive stress distributions on the adhesive and adherend properties are also investigated in the finite element analysis. Since the adhesive is assumed isotropic in the analysis, the equation $G_o = E_o/2(1 + \nu_o)$ holds. For convenience, E_o is used as one of major parameters. The adhesive stress distributions in Figure 10 illustrate the variation of distributions with the change of the elastic modulus ratio of adhesive and adherend (E_o/E_s). The adhesive shear stress shown in Figure 10(a) indicates that the smaller the elastic modulus ratio, the more uniform the adhesive shear stresses. There are two positions, $x = +/-0.6c$, where the adhesive shear stress is equal to the average adhesive shear stress. These two positions are insensitive to the change of the elastic modulus ratio. The adhesive longitudinal (σ_{xo}) and transverse (σ_{yo}) normal stress distributions in Figures 10(b) and (c) also vary with the change of the elastic modulus ratio. For these three adhesive

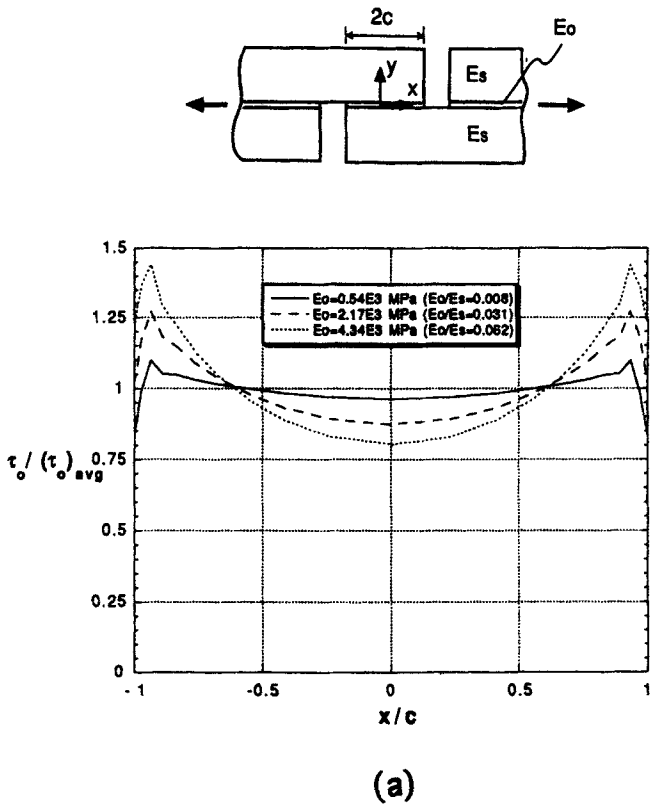

FIGURE 10 The effect of the adhesive elastic moduli on (a) adhesive shear stresses, (b) adhesive longitudinal normal stresses and (c) adhesive transverse normal stresses.

stress components, the higher elastic modulus ratio gives the higher stress concentration near or at the ends of the overlap.

The adhesive shear stress state at the center point of the bond line can be described as a function of the average adhesive shear stress using the correction factor (CF). That is, $\tau_o = \mathrm{CF}(\tau_o)_{\mathrm{avg}}$. The CF *vs.* the elastic modulus ratio (from 0 to 1) is shown in Figure 11, determined from the finite element analysis. It can be seen that the CF decreases from 1 to 0.625 as the elastic modulus ratio (E_o/E_s) increases from 0 to 1. When the elastic modulus ratio equals 1 (representing the specimen without a soft adhesive layer, as in the dummy specimen), the specimen suffers from the highest non-uniformity of the stress distribution

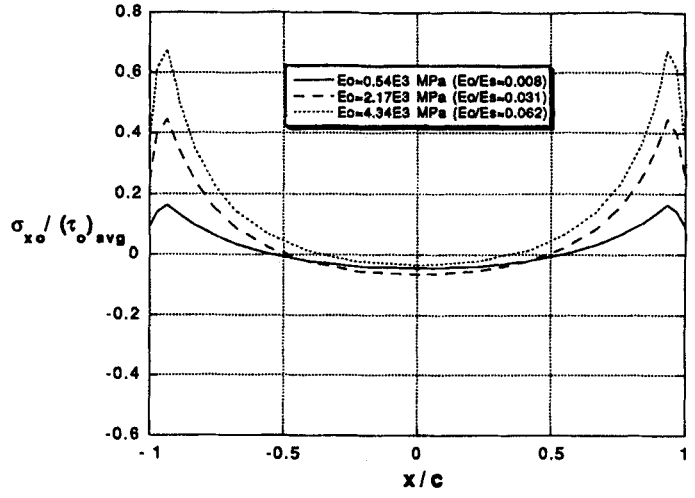

(b)

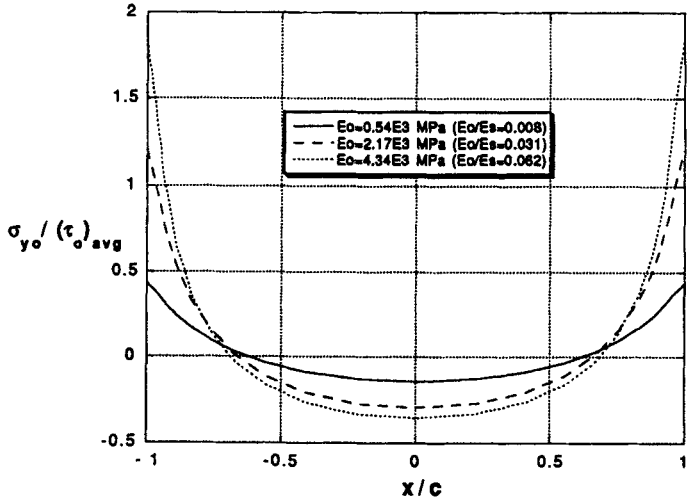

(c)

FIGURE 10 (Continued).

along the bond line. However, as the elastic modulus ratio approaches 0, the stress distribution is almost uniform.

Since the CF can be used to correct the non-uniformity of the adhesive shear stress distributions in the experimental measurement of adhesive shear moduli [5,6], the sensitivity of the CF to the elastic modulus ratio is discussed. In order to correlate the CF to the elastic modulus ratio, a curve-fitting procedure is applied to the data obtained from the finite element analysis. Figure 12(a) shows that the data can be simply and reasonably represented by the equation,

$$\mathrm{CF} = 0.6082 - 0.1704 \log(E_o/E_s) \tag{1}$$

which is limited to the range from $E_o/E_s = 0.008$ to 1 due to the limited data fitting. Thus, Equation (1) cannot describe CF as $E_o/E_s < 0.008$, especially for $E_o/E_s = 0$. From Equation (1), the value of $(E_o/E_s + d(E_o/E_s))$ corresponds to the value of (CF + dCF), *i.e.*

$$\mathrm{CF} + d\mathrm{CF} = 0.6082 - 0.1704 \log(E_o/E_s + dE_o/E_s)) \tag{2}$$

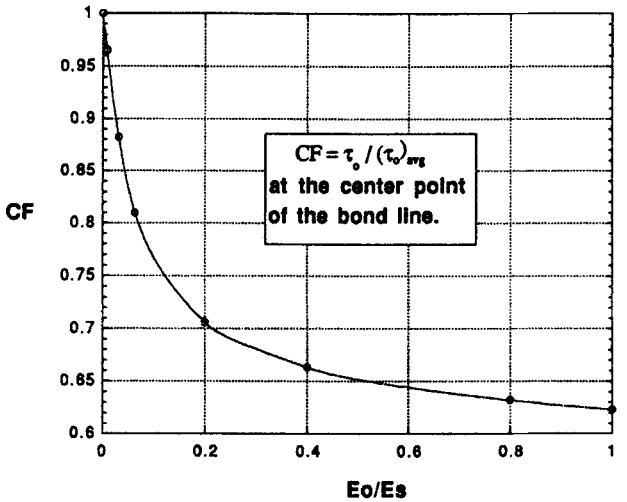

FIGURE 11 The correction factors (CF) for the adhesive shear stress (or strain) at the center point of the bond line, due to the non-uniformity of adhesive shear stress (or strain) distributions for $t/\eta = 62.5$, $2c/t = 1$.

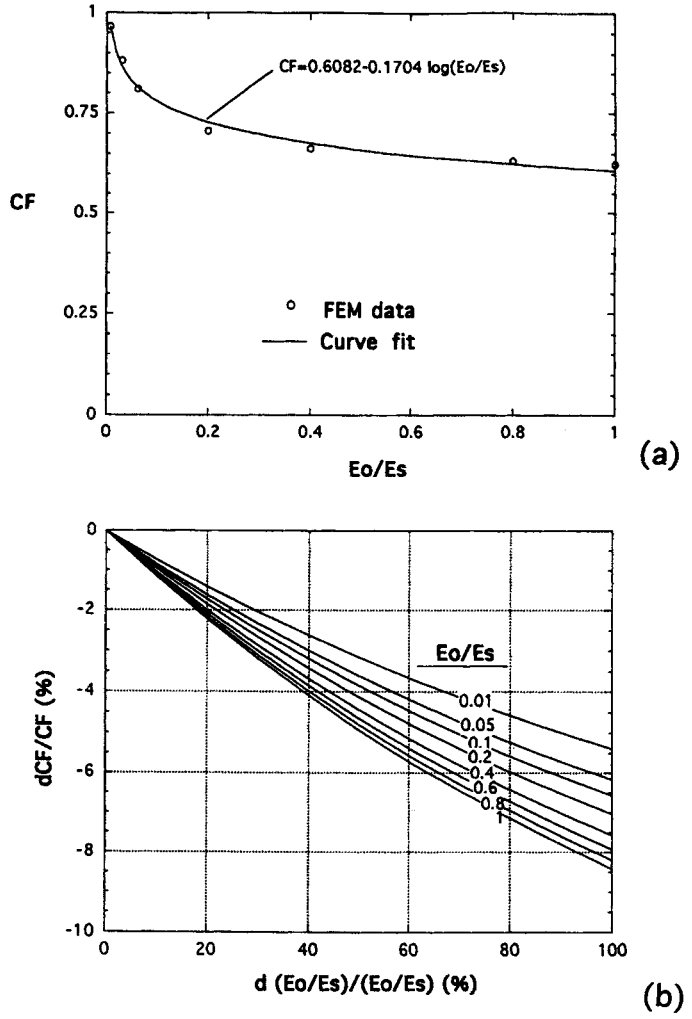

FIGURE 12 (a) Curve fit for correction factors (CF) from numerical data, (b) variation of CF *vs.* variation of ratio of adhesive and adherend elastic modulus.

where d denotes the variation. By subtraction of Equations (1) and (2), the equation can be reduced as

$$dCF = -0.1704 \log\left(1 + \frac{d(E_o/E_s)}{E_o/E_s}\right) \tag{3}$$

Dividing Equation (3) by Equation (1), the equation showing the variation of CF *vs.* the variation of E_o/E_s in terms of proportion, can be written as

$$\frac{d\mathrm{CF}}{\mathrm{CF}} = -0.1704 \log\left(1 + \frac{d(E_o/E_s)}{E_o/E_s}\right) \Big/ (0.6082 - 0.1704 \log(E_o/E_s)) \quad (4)$$

Equation (4) is plotted in Figure 12(b) as $d\mathrm{CF}/\mathrm{CF}$ against $d(E_o/E_s)/(E_o/E_s)$ for $E_o/E_s = 0.01$ to 1. It is shown that the variation of CF is insensitive to the change of E_o/E_s for $E_o/E_s < 1$. The smaller E_o/E_s is, the less sensitive the proportion of the variation of CF is to the proportion of the variation of E_o/E_s. It can be seen that for $E_o/E_s < 1$, a 50% change for the value of E_o/E_s reflects less than 5% variation for the value of CF. Even for a 100% change in E_o/E_s, the CF changes by less than 8%.

The adhesive thickness effect on the adhesive stress distributions has not been analyzed here, but an insight into this effect can be gained by considering the classical solutions for single-lap joints such as Volkersen [9], and Goland and Reissner [8]. From either Volkersen's (shear lag model) or Goland and Reissner's model (assuming the adherends as cylindrical bent plates), it is shown that given a ratio of the overlap length to the adherend thickness ($2c/t$), the adhesive shear stress distribution can be described by a single parameter $(E_o t)/(E_s \eta)$. Although the curve for CF *vs.* E_o/E_s, shown in Figure 11, is for $t/\eta = 62.5$, and $2c/t = 1$, this curve still can be used in the prediction of the CF for different adhesive thicknesses. The E_o/E_s in the horizontal axis can be changed to $(E_o t)/(E_s \eta)$, and the range of the values are replaced from 0 to 62.5, rather than from 0 to 1. The curve for CF *vs.* $(E_o t)/E_s \eta)$ can be applied for various thicknesses of adhesive.

CONCLUSIONS

A simple two-dimensional linear-elastic finite element model has been proposed and validated by comparing it with a moiré experiment. The available classical theories (Volkersen, Goland and Reissner) were also employed to compare the present results. It has been shown that assumptions used in the theories could not be applied to the present

problem and result in a discrepancy with numerical and experimental solutions. The stress fields in the test section for the test specimen with and without load eccentricity have been determined. The load eccentricity highly affected the adhesive stress distribution, but not the stress state at the center point of the bond line. The load eccentricity could result in changes in the adhesive stress concentration which might affect adhesive failure strength determination. The adhesive stress distributions were also influenced by the adhesive/adherend elastic modulus ratio. Correction factors for accounting for the non-uniformity of the adhesive shear stress distributions were determined and used to correct the experimental data measured at the center point of the bond line during the adhesive shear modulus measurement.

Acknowledgment

Financial support from the Federal Aviation Administration under the contract USDOT/FAA 93-G064 is gratefully acknowledged.

References

[1] Krieger, R. B., *Stiffness Characteristics of Structural Adhesives for Stress Analysis in Hostile Environment*, American Cyanamid Co. Havre de Grace, Maryland (1975).
[2] Krieger, R. B., "Adhesive Bonding Design and Analysis," *Engineering Materials Handbook*, Vol. 3 (ASM International, Metals Park, OH, 1990), pp. 459–470.
[3] Hart-Smith, L. J., "Rating and Comparing Structural Adhesives: A New Method," *Engineering Materials Handbook*, Vol. 3 (ASM International, Metals Park, OH, 1990), pp. 471–476.
[4] Kassapoglou, C. and Adelmann, J. C., "KGR-1 Thick Adherend Specimen Evaluation for the Determination of Adhesive Mechanical Properties," *SAMPE Quarterly*, pp. 19–27 (Oct. 1992).
[5] Tsai, M. Y., Morton, J., Krieger, R. B. and Oplinger, D. W., "Experimental Investigation of the Thick-Adherend Lap Shear Test", *J. Adv. Mater.* 28–36 (1996).
[6] Tsai, M. Y., Morton, J. and Oplinger, D. W., "In Situ Determination of Adhesive Shear Moduli Using Strain Gages," *Experimental Mechanics* (in press).
[7] ABAQUS, Finite Element Code, Hibbitt, Karlsson and Sorensen, RI, USA (1992).
[8] Goland, M. and Reissner, E., "The Stresses in Cemented Joints," *J. Appl. Mech.* **11**, A17–A27 (1944).
[9] Volkersen, O., "Die niektraftverteilung in zugbeanspruchten mit konstanten laschenquerschritten," *Luftfahrtforschung* **15**, 41–47 (1938).
[10] Tsai, M. Y., Oplinger, D. W., and Morton, J., "Improved Theoretical Solutions for Adhesive Lap Joints," submitted to *Int. J. Solids and Structures.*
[11] Williams, M. L., "Stress Singularity Resulting from Various Boundary Conditions in Angular Corners of Plates in Extension," *J. Applied Mech.* **19**, 526–528 (1952).